AO12: Exploring Shipping-Induced Aerosol Influence on Cloud Evolution with Geostationary Satellites

Candidate Number: 1056312
Supervisors: William Jones, Peter Manshausen, Philip Stier

Abstract

Aerosol-cloud interactions represent the largest uncertainty in anthropogenic climate forcing, which affects future climate projections. These climate projections would benefit from more detailed input parameters regarding the onset and relaxation times of aerosol-induced changes in cloud properties. Here, the hypothesis that these onset and relaxation times vary with the local solar time of aerosol introduction (a so-called 'diurnal cycle'), is explored. Geostationary satellite retrievals of cloud properties and GPS locations of ships from 2019 were used to track the evolution of polluted clouds directly. The results do not allow rejection of the hypothesis that a diurnal cycle exists, as the nighttime retrieval quality is too low for meaningful deductions. While this work provides valuable insights into the potential existence of a diurnal cycle in aerosol-cloud interactions, further investigations are warranted. Future research should overcome data limitations by collating additional years of satellite observations, with the hopes of providing these more accurate input parameters for future climate projections.

1 Introduction

1.1 Formation of Clouds

Clouds form when water vapour is carried from the surface in rising air parcels, which cool and allow liquid water droplet formation. The condensation of water vapour occurs via nucleation, where a cluster of a now thermodynamically stable phase (liquid water) forms out of the metastable phase it was previously in [1]. The presence of nucleation sites, which could be small naturally occuring particles, 'kickstarts' this process, lowering the concentration of water molecules in vapour phase required by orders of magnitude. Herein, these nuclei will be referred to as aerosols, meaning particles suspended in some fluid (in our case, the atmosphere).

Typically, these aerosols are from natural sources, such as dust from arid regions, sea salt, or ecological sources, such as pollen or fungal spores. Human activities can also introduce aerosols into the atmosphere, primarily by burning fossil fuels. This introduces sulfates and soot into the atmosphere in quantities that vary based on the source.

The introduction of additional anthropogenic aerosols alters the properties of clouds that form around them. The formation of a cloud droplet from water vapour is a thermodynamic process that is ultimately driven by the system's desire to minimise its Gibbs Free Energy. Thus, this report begins with a review of the thermodynamics which govern this process.

1.2 Background Thermodynamics

1.2.1 The Clausius-Clapeyron Equation

At the exact point a phase transition occurs, the two phases are in thermodynamic equilibrium with each other. In the case of liquid-to-gas transitions, this manifests as the rate of evaporation of the liquid being equal to the rate of condensation of the gas. In these conditions, we say the vapour is saturated; any additional water vapour will condense into the liquid phase. The rate at which this saturation vapour pressure changes with temperature is given by the Clausius-Clapeyron equation [2]. An approximate solution for liquid-to-gas transitions is given by

$$P_{CC}(T) = P_{CC}(T_0)\,\mathrm{e}^{\left(\frac{L}{R}\left(\frac{1}{T_0}-\frac{1}{T}\right)\right)} \tag{1}$$

where L [$\mathrm{J\,kg^{-1}}$] is the (assumed constant) latent heat of the phase transition and R [$\mathrm{J\,kg^{-1}\,K^{-1}}$] is the specific gas constant. Here, P_{CC} is the saturation vapour pressure of the water vapour directly above a flat surface of pure water.[1]

In the case of forming water droplets in clouds, we are not considering equilibrium between a flat water surface and vapour above, but instead between water vapour and a collection of droplets of a given radius. This increases the amount of water vapour that can exist in the gaseous phase at the point of equilibrium. This is because water evaporates more readily from a curved surface. This enhanced evaporation means that the saturation vapour pressure above the droplet surface must be higher for condensation to equal evaporation at a given temperature.

[1] For a more thorough recap of Clausius-Clapeyron, see appendix A.

The saturation vapour pressure of water around a collection of droplets of radius r is given by the Kelvin equation [1]

$$P(r,T) = P_{CC}(T)\,\mathrm{e}^{\left(\frac{a}{r}\right)} \tag{2}$$

where a is proportional to surface tension σ [$\mathrm{J\,kg^{-1}}$] divided by temperature T. As equation (2) is asymptotic for $r \to 0$, if this was the full picture then droplet formation would not be possible in the Earth's atmosphere. In the absence of a surface to condense onto, the actual saturation vapour pressure of water in the atmosphere can be far higher than P_{CC}.

1.2.2 Köhler Theory of Droplet Formation

Fortunately, other effects can reduce the saturation vapour pressure necessary for cloud droplet formation. Namely the liquid phase being impure, mixed with some solute. The presence of a solute reduces the number of molecules at the droplet surface and, hence, the rate of evaporation. This leads to a lower saturation vapour pressure. The reduction in saturation vapour pressure is described by Raoult's Law.

In the case of droplet formation, this process is modelled by imagining a set of fixed, soluble aerosols, around which droplets form. As the droplet gets larger, the effect of the aerosol will be diminished. Hence, one would expect condensation nuclei to greatly lower the pressure at which droplets can form, but their effect should diminish as the droplets get larger. The Kelvin equation and Raoult's Law are collected in the Köhler Theory of droplet formation [1], where:

$$P_{aer}(r,T) = P_{CC}(T)\left(1 - \frac{b}{r^3}\right)\mathrm{e}^{\left(\frac{a}{r}\right)}. \tag{3}$$

Here, b is a constant relating to the properties of the aerosol, including molecular mass and number of molecules. This is normalised by the volume of the droplet, as a way to quantify the dilution of the condensation nuclei. $P_{aer}(r,T)$ is the vapour pressure at which droplets of a radius r are in equilibrium. Figure 1 shows a plot of equation 3.

We see that the presence of aerosols greatly lowers the vapour pressure required for equilibrium with droplets of a given radius. Physically, this means that the initial barrier to forming droplets has been lifted by aerosols. Droplet formation at saturation vapour pressures only slightly higher than those over a flat surface of water is now permitted.

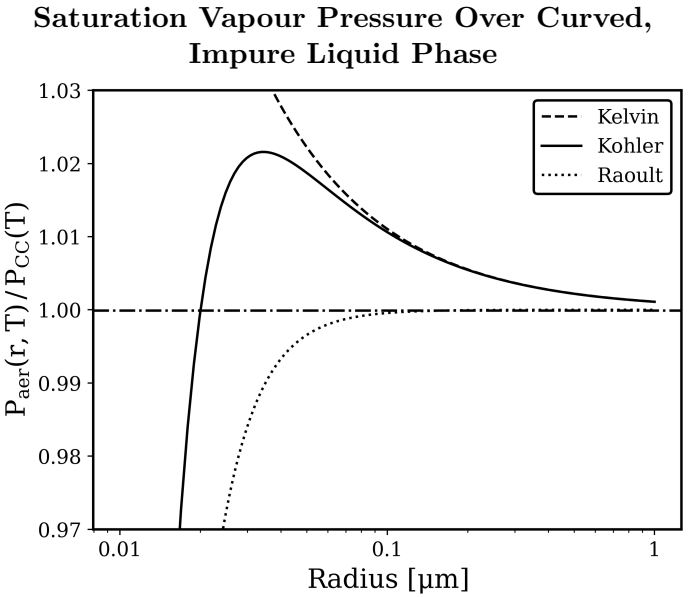

Figure 1: Dashed line shows vapour pressure required to be in equilibrium with a pure water droplet of radius r. The dotted line shows how vapour pressure varies as the radius of the droplet around a fixed aerosol changes. The solid black line is the combination of these two effects.

1.3 Aerosol-Cloud Interactions

A cloud which formed in the presence of additional aerosols will have different properties to a cloud which did not. A first-order effect of aerosol introduction is a reduction in the mean droplet radius. This occurs as a given volume of water is now spread across a larger number of droplets. As explained by Twomey [3], this decrease in mean droplet radius has the effect of giving a cloud a brighter, whiter appearance. There are also second-order effects to clouds, including a lifetime effect [4] where it has been speculated that this reduced effective radius leads to an increase in cloud lifetime. Along with a lifetime effect, another possible second-order effect includes an increase in the liquid water path [$\mathrm{g\,m^{-2}}$] of the cloud. When added to already-formed clouds, aerosols still lower the mean droplet radius by changing the properties of new droplets that are formed.

1.4 The Effect of Clouds on the Global Energy Balance

Clouds affect the global energy balance in multiple ways. Firstly, by increasing the Earth's mean reflectance (albedo), they reduce the solar energy incident on the surface, leading to a cooling effect. Secondly, clouds affect the outgoing longwave radiation emitted from the Earth's surface. Water droplets, being strong absorbers of infrared radiation while in the liquid phase, cause the presence of clouds to reduce the effective emission temperature of the Earth. This reduces the energy radiated by the Earth, leading to a warming effect.

Hence, clouds can have a climactic warming or cooling effect, depending on the relative magnitudes of these two processes.

On average, in high altitude (8–10 km) ice phase clouds, the warming effect is larger. However, in low altitude (< 2 km) clouds, the cooling effect is larger [5].

1.4.1 Anthropogenic Aerosol Effects

Burning fossil fuels introduces both aerosols and greenhouse gases into the atmosphere. Aerosol introduction, via stimulating cloud droplet formation, increasing cloud albedo and potentially increasing cloud lifetimes, negates some of the warming caused by greenhouse gases. The introduction of aerosols at the surface most strongly affects low-altitude clouds, which are known to have an overall cooling effect on the climate [5]. Most recent estimates carried out by the Intergovernmental Panel on Climate Change (IPCC) put the combined forcing of aerosols at $-1.3 \pm 0.7\,\mathrm{Wm}^{-2}$, at a 90% confidence interval [6]. A significant portion of this uncertainty comes from lacking a full understanding of the temporal effect of introduction of anthropogenic aerosols into clouds. This uncertainty could be reduced if there was a more thorough understanding of the onset of these effects in various settings. Of particular importance is uncovering a diurnal (day and night) cycle, where the changes of cloud properties take differing amounts of time to onset depending on the local solar time of aerosol introduction. This collection of onset and relaxation times could then be used as inputs into more sophisticated climate models, which would benefit from knowing the timescales in which changes in cloud properties occur.

In the pursuit of narrowing the error bars on aerosol climactic forcing and hence future climate projections, one may be motivated to intentionally add aerosols to the atmosphere. This would allow researchers to study how cloud properties change in various conditions. However, due to the damaging health effects of aerosols [7], this deliberate intervention raises ethical concerns. As such, an experiment of this type has never been done. Instead, studies focus on settings where aerosols would be introduced to the atmosphere regardless, and use these to analyse the interactions. We refer to this method of studying interactions as 'opportunistic experiments'. It is this type of experiment that forms the basis of the following analysis.

1.5 Opportunistic Experiments

There are many avenues for exploring aerosol-cloud interactions, with each potential aerosol source offering unique benefits. These aerosol sources can be localised, as well as one-off events, such as volcanic eruptions or forest fires. They can also be point sources of prolonged duration, such as industrial sources. While valuable sources of information, these opportunistic experiments offer lower reproducibility, with no ability to control for other factors such as seasonal variations or local cloud regimes. This report focusses on a type of experiment which offers both the opportunity to repeat measurements, and also investigate effects in a variety of settings. Therefore, this investigation relies on emissions from shipping in the oceans as the source of aerosol perturbation.

As a ship moves through the ocean, it introduces aerosols into an otherwise unperturbed cloud bed. First noticed in images from NASA's TIROS-VII, these perturbed clouds can appear as long, continuous bright regions as seen in figure 2.

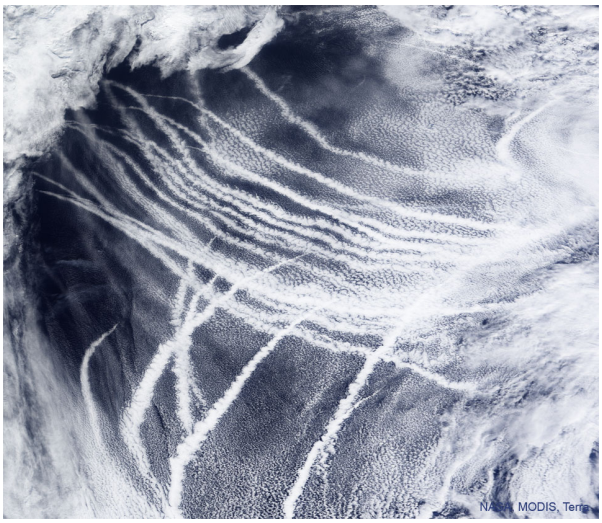

Figure 2: Satellite image showing a possible effect on clouds due to aerosol introduction by shipping. Taken by the MODIS instrument onboard polar-orbiting satellite Terra [8].

Here, we see a situation where the air was likely subsaturated with respect to the natural aerosols available. However, once anthropogenic aerosols were introduced, this lowered the saturation vapour pressure and allowed droplet formation. Herein, these linear, white features will be referred to as 'visible ship tracks'. Visible ship tracks were first detected in 1966, and their origin was put on a firm theoretical footing by Twomey in 1968 [3].

1.6 Prior Work

With satellite images showing visible ship tracks, knowledge of local winds, and GPS locations of ships in the area, a given track can be matched to the ship which caused it. On any given ship track, the time evolution of the properties of polluted clouds can be studied directly. Take figure 2 for example; the narrower ends of the ship track were more recently emitted than the broader, more dispersed ends. Using GPS locations of ships, it can be inferred that the aerosols which were introduced at the narrow end were emitted two hours

ago, but the ones towards the back of the track were emitted 20 hours ago. This means that along any given ship track, by using distance along the track, changes in cloud properties can be measured against time [9].

For use in previous work on aerosol-cloud interactions, the collection of a set of visible ship tracks was done by eye. This was done using images from the Moderate Resolution Imaging Spectroradiometer (MODIS), an instrument onboard a pair of polar-orbiting satellites, Aqua and Terra. As the ship tracks were detected using MODIS, analysis of their properties was also done using retrievals from these instruments. This pair of instruments provides images of each point on the Earth's surface every 12 hours. This means that only two observations of any given ship track can be made before its effects are too diffuse to follow.

Until recent work by Manshausen et al., the investigation of ship tracks relied on visual detection [10]. Manshausen argues this introduces a sampling bias; in a global fleet of order 10^5 ships, only 100s – 1000s of ship tracks could be identified per year. Hence, results are biased towards studying aerosol perturbations in clouds where conditions allow visible ship track formation. Manshausen demonstrates that even in the absence of a visible ship track, the properties of the cloud are still altered by aerosol introduction. Manshausen's work used GPS locations of ships, along with local winds, to track the polluted clouds along their paths, rather than visually identifying the motion of the tracks. Whilst Manshausen's work mitigates the requirement to use MODIS, he still opted to use these instruments for his analysis. This means that whilst his work benefits from the larger amount of ship tracks to study, it is still constrained by a small number of measurements per track.

It has been demonstrated with MODIS retrievals that the peak change in cloud droplet effective radius occurs around 3 hours after the emission of aerosols at the surface [10]. It has also been noted that there is a weak average change in the liquid water content of clouds which are polluted with anthropogenic aerosols [11]. The 3-hour onset time for these maximal effects is an average over the entire day, and current research has not yet been able to uncover a variation in the onset and relaxation time of these effects with local solar time.

1.7 This Report

As Manshausen's work mitigated the requirement to use the MODIS instruments, this work takes advantage of this by using an instrument with higher time resolution. This project uses data from the Spinning Enhanced Visible and Infrared Imager (SEVIRI) onboard the Meteosat Second Generation (MSG) geostationary satellite. MSG, originally a weather forecasting satellite, has been long overlooked as an avenue for exploring the temporal evolution of cloud properties. While offering lower spatial resolution compared to low-Earth polar orbitting satellites, this alternative substantially advances time resolution. With images of the Earth taken every 15 minutes, the evolution of polluted tracks can be directly tracked, rather than observing them in snapshot images. Along with allowing changes in the clouds close to the aerosol introduction to be accounted for, this vastly increases the mass of data available for study. It is hoped that this reduced error and larger dataset will help uncover a diurnal cycle.

Attention is focused on a particular cloud type, marine stratocumulus. These are low altitude (1–2 km), typically liquid phase clouds [1] found over oceans. These are of particular importance for two reasons; they cover about 20% of the Earth's oceans, and they have been shown to have the highest sensitivity to aerosol perturbations [12]. In this report, the mean droplet radius and liquid water content of these clouds is investigated.

Known locations of aerosol emissions were followed along the paths of winds using a Lagrangian approach[2] (hereafter, this process is referred to as advection) and changes in cloud properties were measured against time. This direct introduction of a time axis to measurements allows for studying of cloud properties without a systematic error due to a changing background state. This marks a significant step forward in understanding aerosol-cloud interactions.

1.7.1 Structure of Report

In section 2.1, the process of collecting ship tracks, along with their filtering and generation of background sampling locations is discussed. This is followed by section 2.2 where the advection process is outlined. In section 2.3, the SEVIRI instrument is discussed, including the retrievals it offers, and its spatial and temporal resolution. The methods section is concluded by 2.4, where the experiments carried out on the collection of ship tracks are detailed. The outcomes of these experiments are collected in section 3, and in section 4.2 these outcomes are interpreted and compared to that of previous work. Section 4.3 contains recommendations for future research.

2 Methods

2.1 Emissions Dataset and Measurements of Background

The analysis began with an input dataset of ship locations, which was compiled using Automated Identifica-

[2] a Lagrangian approach to fluid mechanics means centering a coordinate system on a moving parcel of fluid.

tion Systems (AIS) [13]. A given AIS 'location' contains a latitude-longitude pair, along with a time that the ship was there. The AIS method of ship identification has high spatial accuracy, identifying ship locations within a few tens of metres [14]. Along with mitigating the sampling bias identified in Manshausen, using AIS offers a vast increase in the number of ship tracks available for study. Prior work studying visible ship tracks over multiple years has been limited to a few thousand tracks [10] whereas for 2019 alone there are of order 10^6 to consider.

The locations given by AIS were grouped together into 'ship tracks' using Python's 'Trackpy'. This tracking algorithm had a tendency to group points non-physically in ways that a real ship could not move. Non-physical groupings included two distinct ship tracks being joined, which may have been travelling on entirely different bearings or simply over-fitted noise of random locations. The first step of data cleaning involved removing these non-physical tracks.

2.1.1 Filtering Ship Tracks

The first filter applied to ship tracks was a length filter; all ship tracks which were made up of less than 10 AIS locations were removed. To each ship track of length 10 or greater, a fitting process was applied with a second-order polynomial using the 'polyfit' package from NumPy. This was done with longitude being mapped to x and latitude being mapped to y on a linear tangent plane. Subsequently, a least squares analysis was conducted using NumPy's 'corrcoef' to assess the goodness of fit. Ship tracks with an R^2 value below 0.97 were classified as 'bad ship tracks'. To these 'bad ship tracks', x and y were exchanged and the process was repeated. This was done to mitigate the possibility of removing valid groups of locations which happen to be multi-valued in longitude. All tracks which did not pass either goodness of fit test were excluded from all subsequent analyses. This new collection of paths is herein referred to as our 'good ship tracks'.

2.1.2 Generation of Sampling Points

To decouple natural variations in cloud properties from those due to aerosol influence at each location, the background cloud state is also measured. This enables us to make valid comparisons of changes in cloud properties. In order to make this comparison, a latitude-longitude pair is required which is near the AIS location, but far enough away to not be affected by the introduction of aerosols. These points were generated by making use of our fitted ship tracks. For each track, sampling points were generated as though there was a ship on either side of the real ship, travelling at an instantaneously parallel bearing. Computationally, this was done by evaluating a unit vector orthogonal to the heading of the ship at each of the fitted points, and travelling 30km in each direction.[3] In figure 3, we see an example of four of these fitted ship tracks.

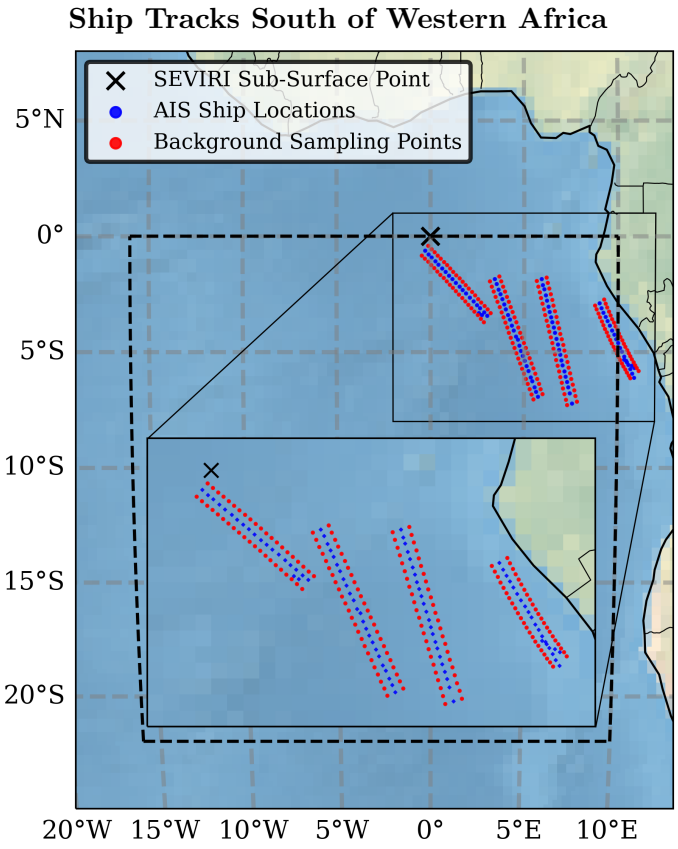

Figure 3: Four example ship tracks, where blue dots indicate actual ship locations, according to AIS. The red dots are the generated sampling points of background clouds. The black cross is the point on the Earth's surface directly below the geostationary satellite used, SEVIRI. The outer black dashed line is the region in which we are considering ship tracks, chosen because it contains large decks of marine stratocumulus clouds, which are very important for the global energy balance.

Figure 3 also shows an erroneously grouped 'ship track', the rightmost ship track on the inset map. Towards the southern end of the track, we can see what appears to be a second ship crossing over, joined onto the same track. There were some tracks of this type that passed the fitting procedure but do not actually represent physical tracks.

Generation of sampling points before distortion of the ship tracks by winds (the advection process) is different to the method applied in prior work on this subject. In previous work, including that by Manshausen, a given ship track would be advected with local winds, forming a new, likely more complicated shape [10]. Background sampling points were generated by taking this new collection of locations and translating them by a vector of length 30 km, orthogonal to the ship's bear-

[3] As 1 degree of longitude at the equator is 111 km, this corresponds to a 'distance' of 0.27 units in latitude-longitude space.

ing in both directions. In practice, this can be done by adding and subtracting a fixed latitude-longitude vector to every point as

$$\begin{pmatrix}\text{Longitude}\\ \text{Latitude}\end{pmatrix} \pm \begin{pmatrix}a_i\\ b_i\end{pmatrix} = \begin{pmatrix}\text{Control Longitudes}\\ \text{Control Latitudes}\end{pmatrix}$$

where a_i and b_i depend on the ship track under consideration, along with the current locations of the sampling points.

My reasons for undertaking a different method were twofold. Firstly, picking an area of cloud nearby and following this point gives a fairer reflection of a changing background state. Redefining the chosen control point for each measurement seemed to introduce unnecessary variability into the process. Secondly, this method of fixing spacing before advection would allow monitoring of the extent of spatial disturbances independent of local winds. We can see how the effect spreads over the 30 km spacing by interpolating between the advected AIS (the polluted clouds) and background points, then measuring the cloud properties along that line and plotting as a function of spacing. This type of analysis would be beyond the scope of the dataset if the sampling points were generated at a fixed distance after advection. This type of investigation was not carried out in the end.

2.2 Advection Algorithm

Time evolving the AIS locations with winds is done using the Hybrid Single-Particle Lagrangian Integrated Trajectory (HYSPLIT) model [15]. This model uses European Reanalysis 5 (ERA5) winds. Here, reanalysis refers to the process of using computer models to integrate various observational data sources, such as satellite measurements and weather balloon data, to create a detailed model of the Earth's atmospheric state. These ERA5 winds have a 3-hour time resolution, but the HYSPLIT model interpolates to improve this, providing the time resolution we require. As the changes in cloud properties occur on time scales of order 10 hours, the advection process was carried out for 24 hours. This was done so that both changes in cloud properties and relaxation to a stable, consistent state could be observed.

The 'initial emission height' inputted to the HYSPLIT model was 20 m, as this is the assumed height of the top of the ship's smokestack. Herein, we refer to an original point (AIS or control), and the locations it is advected to as an 'advection trajectory'.

2.3 SEVIRI Retrievals

2.3.1 The SERVIRI Instrument

SEVIRI is an instrument onboard the MSG satellite, operated by the European Space Agency. It is in a geostationary orbit, positioned at a nominal longitude of 0 °, 36000 km above the Gulf of Guinea. It has four viewing channels, spread across the visible and near-infrared, and takes images of the Earth every 15 minutes, with 3×3 km resolution at its sub-surface point. SEVIRI retrievals of cloud properties were calculated using the algorithm laid out by G. R. McGarragh et al. [16]. These retrieved properties were stored on JASMIN group workspaces. There are 96 files for each day of 2019 which were made available for this work. This collection of files will be referred to as 'cloud products'. Cloud products contains retrieved cloud properties and their associated uncertainties, such as cloud top height or liquid water path, along with further information regarding the conditions of the retrievals, such as whether it was daytime, nighttime, or twilight.

2.3.2 Required Retrievals

From the cloud products files, cloud droplet effective radius and liquid water path were retrieved. To focus the investigation on marine stratocumulus as intended, the cloud's phase was also retrieved (filtering only for liquid-phase clouds) and cloud top height, making sure it lies within the range expected for stratocumulus. A complete accounting of retrieved cloud properties, valid ranges of uncertainties, and dimensions is given in appendix B, table 2.

2.3.3 Retrieval Quality at Day, Night and Twilight

The retrieval algorithm suffers at nighttime, as it is limited to only infrared channels. This algorithm also suffers at twilight, where the solar zenith angle is large. It does not deal well with the refraction of visible light in droplets. This leads to large errors in stated values, even if the quoted uncertainties remain small [16], especially at twilight.

2.4 Point Filtering Experiments

The SEVIRI retrievals have a far lower signal-to-noise ratio than satellites used in similar work on this subject. This is in part due to it being much further away from the Earth, and also because this type of analysis is different from the intended purpose of this instrument. Hence, further steps were taken to strengthen this signal. Three different methods of improving the signal-to-noise ratio were investigated. The first approach involves a reduction of noise, omitting points from the analysis whose uncertainties were above cutoff values. The latter two approaches involve increasing the strength of the signal by only sampling polluted clouds whose properties are expected to differ the most from the background state. Firstly this was done by attempting to reintroduce the visible ship track sampling bias. The second approach involves only including the most polluting ships in the global fleet.

2.4.1 Point-Wise Filtering

For each location cloud property retrievals were required, this was matched it to the nearest available pixel in SEVIRI. The cloud properties given in appendix B were recorded. In point-wise filtering, we impose that all of these recorded values and their uncertainties fall in a reasonable range. If one of the values is not in a reasonable range, then this pixel's values were not included for other measurements. For example, if the given droplet effective radius is of order 100 µm (which is large compared to a typical average droplet radius of order 5 µm), all measurements from this pixel are omitted.

Although retrievals of differing properties (e.g. droplet effective radius and cloud height) are largely independent, the rationale behind this approach is that low quality in one value implies reduced confidence in the accuracy of the remaining retrievals, regardless of quoted uncertainties.

2.4.2 Investigating 'Visible Ship Track' Properties

One investigation carried out was into the properties of the type of ship tracks that would have previously been identified when tracks were collected by eye. This requires filtering of the collection of good ship tracks for ones that would have been visible to the human eye. The method chosen for this filtering involved three steps. First, the polluted cloud points and the background points were individually filtered using the same criteria as in section 2.4.1. The second step involved omitting any of the polluted cloud locations which did not keep both of its corresponding background points. The third and final step involved imposing that the albedo (measured in dimensionless units $\in [0, 1]$) of the polluted points differed from that measured at the corresponding background points by at least 0.05. If this condition was satisfied by any point on the advection trajectory of the polluted cloud, the entire trajectory was kept. This was done at any point on the advection trajectory, rather than just the first location where we know the ship was. Cloud properties can take a few hours to be affected by the introduction of aerosols, hence this is allowed for in this filtering process.

2.4.3 Mass of Aerosols Deposited

The set of good ship tracks can also be filtered to include only the most polluting ships in the global fleet. Using the model of Jalkanen et al. [14], vessel type, fuel type, and speed (calculated using subsequent AIS locations) were combined to estimate aerosol deposition into the atmosphere. The exact details of this calculation are beyond the scope of this report. For our purposes, using this model is a way to filter the dataset for the most polluting ships.

Equation 3 tells us how droplets form using aerosols as condensation nuclei. However, without enough aerosols added to the cloud, the measured changes in the properties could be negligible. Experimenting with highly polluting ships provides an avenue to explore the effects without the constraint of the cloud 'running out' of additional aerosols.

3 Results

Except where stated otherwise, measurements of retrieved cloud properties only include daytime retrievals.

3.1 Point-Wise Filtering Results

The results of point-wise filtering are shown in the first row of table 1. This shows a comparison between the cloud properties of droplet effective radius (CER) and liquid water path (CWP). The measured differences in both of these properties were small. This method of filtering led to the largest average droplet effective radius and lowest mean liquid water content. The weak change in liquid water content is in accordance with previous work on marine stratocumulus, but the low average change in droplet effective radius is not [10].

3.2 Albedo Filtering Results

The results of the albedo filtering experiment are shown in the second row of table 1. Filtering according to albedo measurements, more significant differences in CER, but the main difference is in CWP. We separate the deviation of CER by time since emission to investigate a systematic trend in the decrease. This can be seen in figure 4.

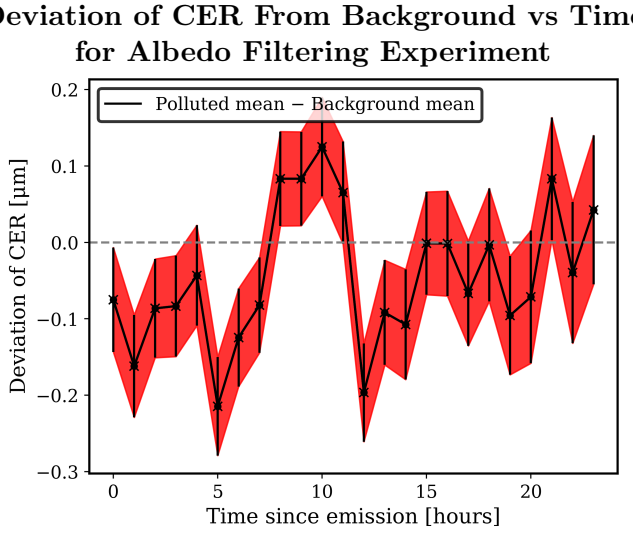

Figure 4: Polluted mean − background mean, separated by hours since emission. The ship tracks collected for this analysis are ones that met the 'visibility' condition laid out in section 2.4.2. The red area is a range of uncertainty, calculated by propagating errors on both the polluted mean and background mean.

Filtering Method	CER [μm]		CWP [$g\,m^{-2}$]	
	Polluted	Background	Polluted	Background
Point-wise Filtering	6.07 ± 0.004	6.08 ± 0.001	18.06 ± 0.006	18.07 ± 0.004
Albedo Filtering	5.03 ± 0.010	5.08 ± 0.013	21.13 ± 0.065	20.02 ± 0.062
Mass Filtering	5.31 ± 0.007	5.40 ± 0.005	20.95 ± 0.039	21.10 ± 0.029

Table 1: Results of each filtering experiment are given in rows 1–3 of the above table. These averages were calculated including only daytime retrievals. For the full plots from which these averages are calculated, see appendix C, figures 7, 8 and 9.

Whilst the distributions of droplet effective radii showed systematic differences, when separated by time since emission there is no discernible pattern. As averaging over 24 hours should recover a maximum deviation around 3 hours after emission, followed by a relaxation to the background, it was concluded that there is a flaw with this method of selecting which ship tracks to include in the analysis. This was validated by the large difference in cloud water path, compared to the expected negligible difference. Hence, no further steps were taken in the analysis of this collection of tracks.

3.3 Mass Filtering Results

The results of mass filtering are shown in the third row of table 1. Filtering for the most polluting ships in the fleet gives the largest difference in the mean droplet effective radius of all experiments conducted. It also successfully recovers the expected weak average change in the liquid water content of polluted clouds. Figure 5 shows the deviation of droplet effective radius vs time since emission.

Deviation of CER From Background vs Time for Mass Filtering Experiment

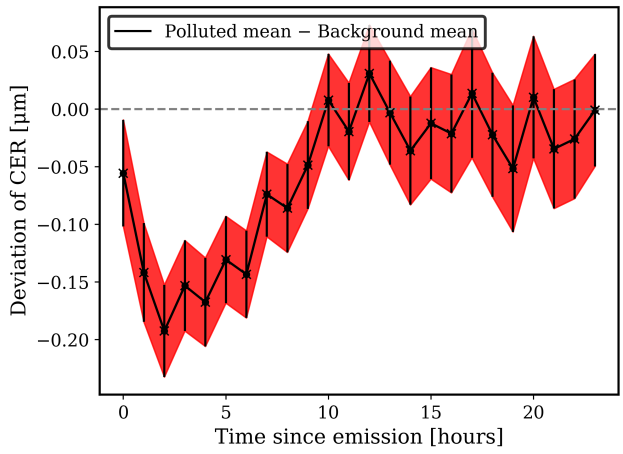

Figure 5: As in figure 4, this is polluted mean − background mean, separated by hours since emission. This plot only considers the most polluting ships in the global fleet.

We see an average decrease before tending back to background, with the maximum effects seen between 2–4 hours after emission. There is a measured relaxation time of around 10 hours. Both of these findings are in agreement with current literature [17].

A second-time dimension was then incorporated, separating further by an hour of emission. This can be seen in figure 6 where, for completeness, nighttime retrievals are also included.

Deviation of CER From Background vs Time and Time of Emission for Mass Filtered Data

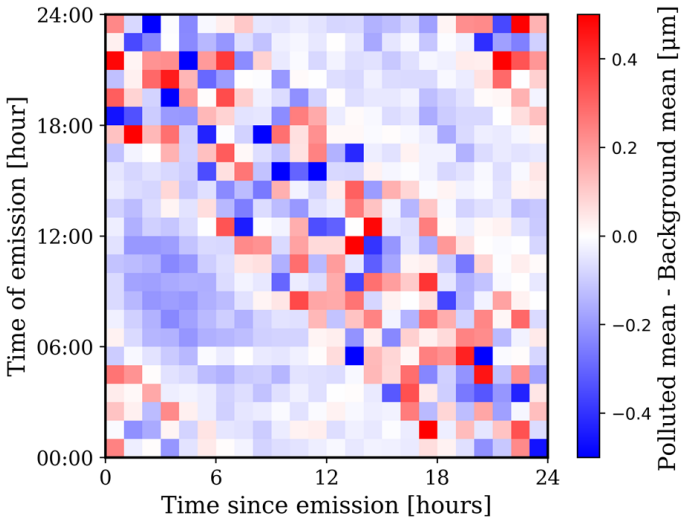

Figure 6: Local solar time of emission (y-axis) vs time since emission (x-axis). This is figure 5, separated into 24 separate plots, one for each hour of emission of the day. The value of polluted mean − background mean can be found by comparing the colour of a given pixel to that of the colour bar. A time of retrieval can be obtained by summing the x and y axes values. The diagonal regions represent retrievals done at nighttime, where the retrieval quality is lower.

In the light blue diagonal band, which originates for a time of emission between 06:00 and 18:00, we see what is expected: an average lowering of mean droplet effective radius inside of the clouds within a few hours. This is the small dark blue region that can be seen in this light blue diagonal band. Outside the daytime bands, the signal-to-noise ratio is too low for any meaningful interpretation.

4 Conclusion

4.1 Systematic Differences Between Outcomes of the Sampling Methods

In table 1, the CER value for the point-wise method of filtering is far larger than in both albedo filtering and mass filtering. The presumed origin of this effect is an indirect spatial sampling bias in the latitude-longitude region of consideration. The region, depicted in figure 3, contains a shipping corridor. This is on a roughly straight line between the westernmost point of Africa, and South Africa. This area is populated by large freight vessels, which are the ships which deposit the greatest mass of aerosols into the atmosphere. Hence, the method of filtering for the polluting ships also indirectly narrows the region of consideration. This region has been demonstrated to have permanently altered cloud properties thanks to this shipping corridor [18]. Hence the discrepancy in the mass-filtered CER and the pointwise-filtered CER.

Table 1 also shows a large difference in the measured cloud water path of our albedo-filtered dataset. It is assumed that this arose from the method of selecting 'visible' ship tracks. The intention for the albedo filter was to select clouds with smaller droplet effective radius, which have a higher albedo due to the Twomey effect discussed in section 1.3. It instead appears as though the method biased thicker clouds with more liquid water. These thicker clouds tend to scatter (and hence reflect) light more effectively, leading to a higher albedo than thinner clouds. Hence, this method of reintroducing visibility was unsuccessful.

4.2 Interpretation of Results

The primary goal of this project was to provide more sensitive input parameters for future climate projections. Particularly, uncovering a daily variation in the onset and relaxation times of aerosol-induced changes in cloud properties. Averaged over all hours of the day, polluted clouds have, on average, a lower mean droplet effective radius. This difference is at its greatest between 2–4 hours after the introduction of aerosols, and cloud properties return to that of the background after 10 hours. This is in agreement with previous work on the topic [10]. Advancements were hoped to be made by uncovering a diurnal cycle, where there is a difference in the time it takes to return to the background based on the local solar time of aerosol introduction.

These results do not allow us to reject the hypothesis that a diurnal cycle exists. The relaxation time of cloud droplet effective radius is measured to be 10 hours, and there were no emission times with 10 hours of measurements uninterrupted by the noise from the low-quality nighttime retrievals. It should be noted that, due to one of the filtering conditions being removing points with uncertainties above a certain threshold, this disproportionately removes nighttime measurements. Hence, the noise seen in the diagonal regions is in part due to lower retrieval quality, and also an artifact of a reduced dataset size.

The steps taken in this project have mostly revolved around making 'common sense' reductions to the points we considered with the hopes of improving the signal. This began with the filtering of the ship tracks to remove invalid ones and continued throughout the work, up to the point of only including the most polluting ships. This has had a positive effect on the daytime retrievals and has allowed for a clear signal on the diagonal band of figure 6. However at nighttime, when the retrieval quality is lower, the signal is drowned by noise and is unable to be overcome by sufficient quantities of data.

4.3 Future Work

In lieu of any reason to assume systematic bias in nighttime retrievals, I assume the issue can be mitigated with a sufficient mass of data and less stringent filtering. Whilst this does lower the signal seen during the day, it flattens the noise seen at nighttime. This offers an avenue for the existence of a diurnal cycle to be investigated. Without this mass of data, there will not be a way to uncover a diurnal cycle using SEVIRI.

Hence, I suggest repeating the analysis for multiple years of AIS locations and SEVIRI retrievals, filtering only points to remove those with large uncertainties and those that occur at twilight. The mass filtering method could also be a useful filter, and experimentation with cutoffs that improve signal seen without reducing dataset size too much should be investigated.

References

[1] U. Lohmann et al. *An Introduction to Clouds: From the Microscale to Climate*. Cambridge University Press, Cambridge, 1st edition, 2016.

[2] K. Blundell and S. Blundell. *Concepts in Thermal Physics*. Oxford University Press, Oxford, 2nd edition, 2009.

[3] S. Twomey. The influence of pollution on the shortwave albedo of clouds. *Journal of Atmospheric Sciences*, 34(7):1149–1152, 1977.

[4] U. Lohmann and J. Feichter. Global indirect aerosol effects: a review. *Atmospheric Chemistry and Physics*, 5(3):715–737, 2005.

[5] J. Mülmenstädt, M. Salzmann, J.E. Kay, et al. An underestimated negative cloud feedback from cloud lifetime changes. *Nat. Clim. Chang.*, 11:508–513, 2021.

[6] V. Masson-Delmotte et al. *IPCC Climate Change 2021: The Physical Science Basis*. Cambridge University Press, 2021.

[7] S. Mack, A. Madl, and K. Pinkerton. Respiratory health effects of exposure to ambient particulate matter and bioaerosols. *Comprehensive Physiology*, 10(1):1–20, Dec 2019.

[8] NASA. NASA Astronomy Picture of the Day (APOD), 2022. `https://apod.nasa.gov/apod/ap220608.html`.

[9] E. Gryspeerdt, T. Goren, and T. W. P. Smith. Observing the timescales of aerosol–cloud interactions in snapshot satellite images. *Atmospheric Chemistry and Physics*, 21(8):6093–6109, 2021.

[10] P. Manshausen, D. Watson-Parris, M. Christensen, J. Jalkanen, and P. Stier. Invisible ship tracks show large cloud sensitivity to aerosol. *Nature*, 610(7930):101–106, 2022.

[11] V. Toll, M. Christensen, J. Quaas, and N. Bellouin. Weak average liquid-cloud-water response to anthropogenic aerosols. *Nature*, 572:51–55, 2019.

[12] T. Goren and D. Rosenfeld. Extensive closed cell marine stratocumulus downwind of europe—a large aerosol cloud mediated radiative effect or forcing? *Journal of Geophysical Research: Atmospheres*, 120:6098–6116, 2015.

[13] International Maritime Organisation. Ais transponders. Accessed on 18/04/2024, `https://www.imo.org/en/OurWork/Safety/Pages/AIS.asp`.

[14] J.P. Jalkanen, L. Johansson, J. Kukkonen, A. Brink, J. Kalli, and T. Stipa. Extension of an assessment model of ship traffic exhaust emissions for particulate matter and carbon monoxide. *Atmospheric Chemistry and Physics*, 12(5):2641–2659, 2012.

[15] A. F. Stein, R. R. Draxler, G. D. Rolph, B. J. B. Stunder, M. D. Cohen, and F. Ngan. Noaa's hysplit atmospheric transport and dispersion modeling system. *Bulletin of the American Meteorological Society*, 96(12):2059 – 2077, 2015.

[16] G. R. McGarragh, C. A. Poulsen, G. E. Thomas, A. C. Povey, O. Sus, S. Stapelberg, C. Schlundt, S. Proud, M. W. Christensen, M. Stengel, R. Hollmann, and R. G. Grainger. The community cloud retrieval for climate (cc4cl) – part 2: The optimal estimation approach. *Atmospheric Measurement Techniques*, 11(6):3397–3431, 2018.

[17] M. W. Christensen, A. Gettelman, M. Diamond, P. Stier, et al. Opportunistic experiments to constrain aerosol effective radiative forcing. *Atmospheric Chemistry and Physics*, 22(1):641–674, 2022.

[18] M. Diamond, P. Stier, et al. Substantial cloud brightening from shipping in subtropical low clouds. *AGU Advances*, 1(1):e2019AV000111, 2020.

Appendicies

A Clausius-Clapeyron Intuition

The Clausius-Clapeyron equation reads [2]

$$\frac{dP}{dT} = \frac{L}{T(v_{gas} - v_{liq})} \tag{4}$$

where L [$\mathrm{J\,kg^{-1}}$] is the latent heat of the phase transition. v_{gas} and v_{liq} are the volumes of 1 kg of gas and liquid respectively at this temperature (T) and pressure (P). In the limit of $v_{gas} \gg v_{liq}$, this equation can be solved to recover equation 1. Understanding what this equation tells us is best done with an example. Consider a container of fixed volume at temperature T, which only contains H_2O molecules. In one limit, the molecules are all in a gaseous phase, and the pressure in the container is maximal. In the other limit, the water is all in liquid phase, and there is a vacuum above the water. Both of these states are not in equilibrium; the equilibrium state will have a mixture of each phase, with some pressure at the waters surface due to a certain amount of molecules in gaseous phase. This equilibrium is characterised by evaporation of liquid phase being equal to condensation of the gaseous phase. Clausius-Clapeyron tells us what that pressure of the vapour is, at a given temperature. In some conditions, e.g., very high temperature, the water will all be in gaseous phase, and the pressure this causes will be below the pressure required by Clausius-Clapeyron for equilibrium between the two phases. Here, water vapour exists in equilibrium with itself.

B SEVIRI Retrievals and Filtering Conditions

Flag	Property	Units	Valid Range	Uncertainty	Uncertainty Range
'cer'	Droplet effective radius	μm	$\in$ [0, 40]	'cer_uncertainty'	< 5
'cwp'	Liquid water path	g/m^2	$\in$ [0, 100]	'cwp_uncertainty'	< 10
'cth'	Cloud top height	km	$\in$ [0.5, 2.5]	'cth_uncertainty'	< 0.5
'cot'	Optical thickness	1	$\in$ [0, 40]	'cot_uncertainty'	< 5
'...albedo...'	Albedo in visible	1	$\in$ [0, 1]	'...albedo_uncertainty...'	< 0.2
'illum'	Day, night or twilight	1	integer $\in$ [1, 3]	-	-
'cldtype'	Pavolonis cloud type	1	integer $\in$ [0, 7]	-	-
'lat'	Latitude	$^\circ$	$\in$ [-22, 0]	-	-
'lon'	Longitude	$^\circ$	$\in$ [-16, 10]	-	-

Table 2: Cloud property names ('Flag') as given on SEVIRI cloud products file, with descriptions and dimensions. The valid range of latitude and longitude in relation to SEVIRI's sub-surface point is shown in figure 3. The full name for the albedo flag is 'cloud_albedo_in_channel_no_1', and uncertainty is 'cloud_albedo_uncertainty_in_channel_no_1'

The 'cldtype' flag is an integer between 1 and 7, which tells us the phase of the cloud in the pixel, with '0' reserved for clear conditions. We only consider liquid-phase clouds, fixing 'cldtype' = 3 in all that follows. This was done to focus our investigation on low-altitude marine stratocumulus, which are liquid-phase clouds.

C Cloud Property Histograms

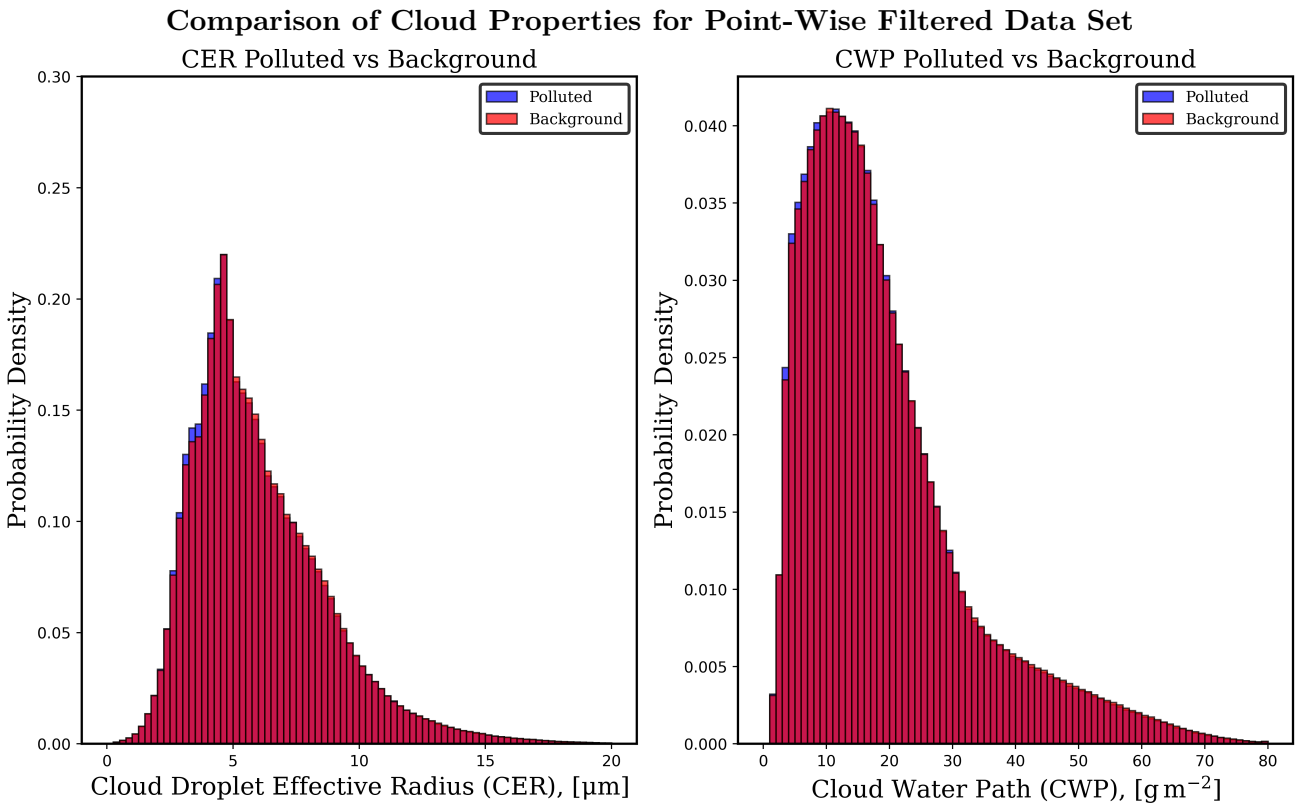

Figure 7: Comparison of polluted cloud properties to the background for the point-wise filtered dataset. Subplots include (left to right) cloud water droplet effective radius and cloud liquid water path.

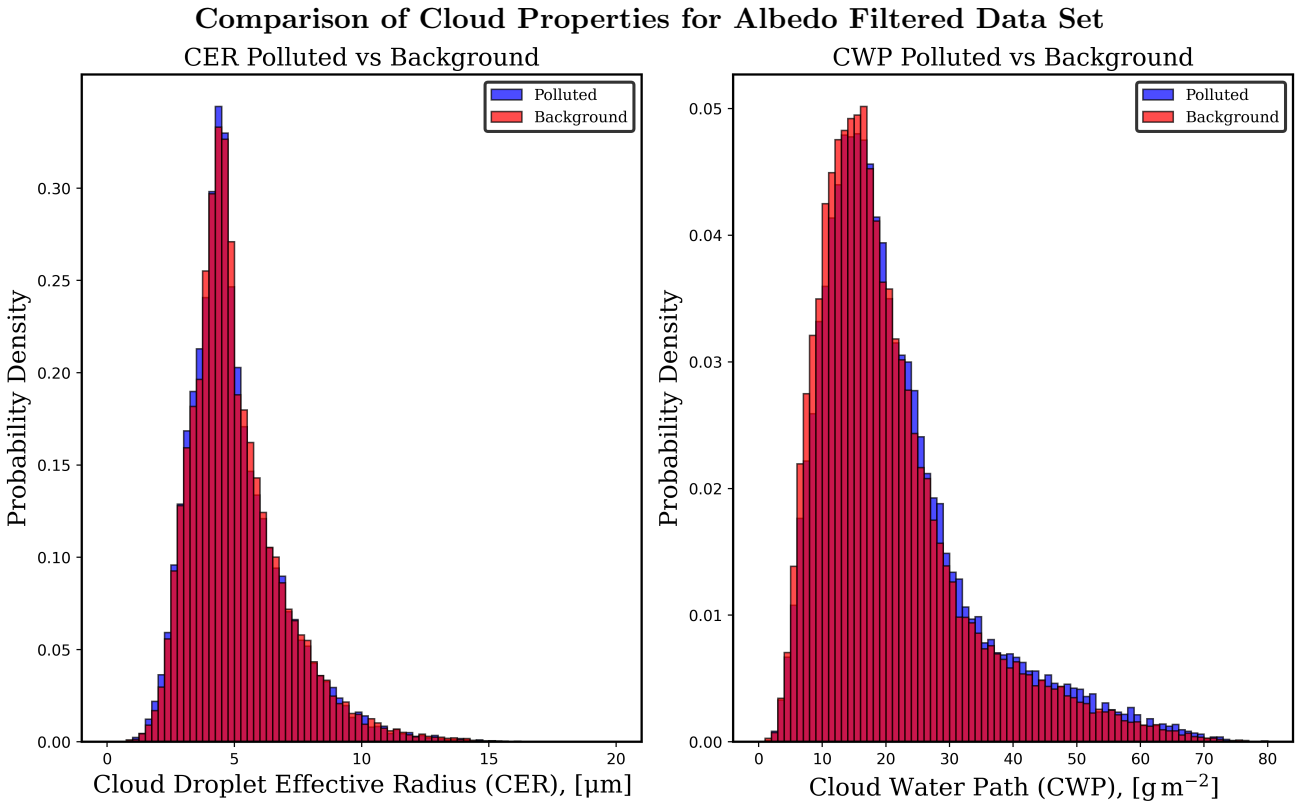

Figure 8: Comparison of polluted cloud properties to the background for the albedo-filtered dataset. Subplots include (left to right) cloud water droplet effective radius and cloud liquid water path.

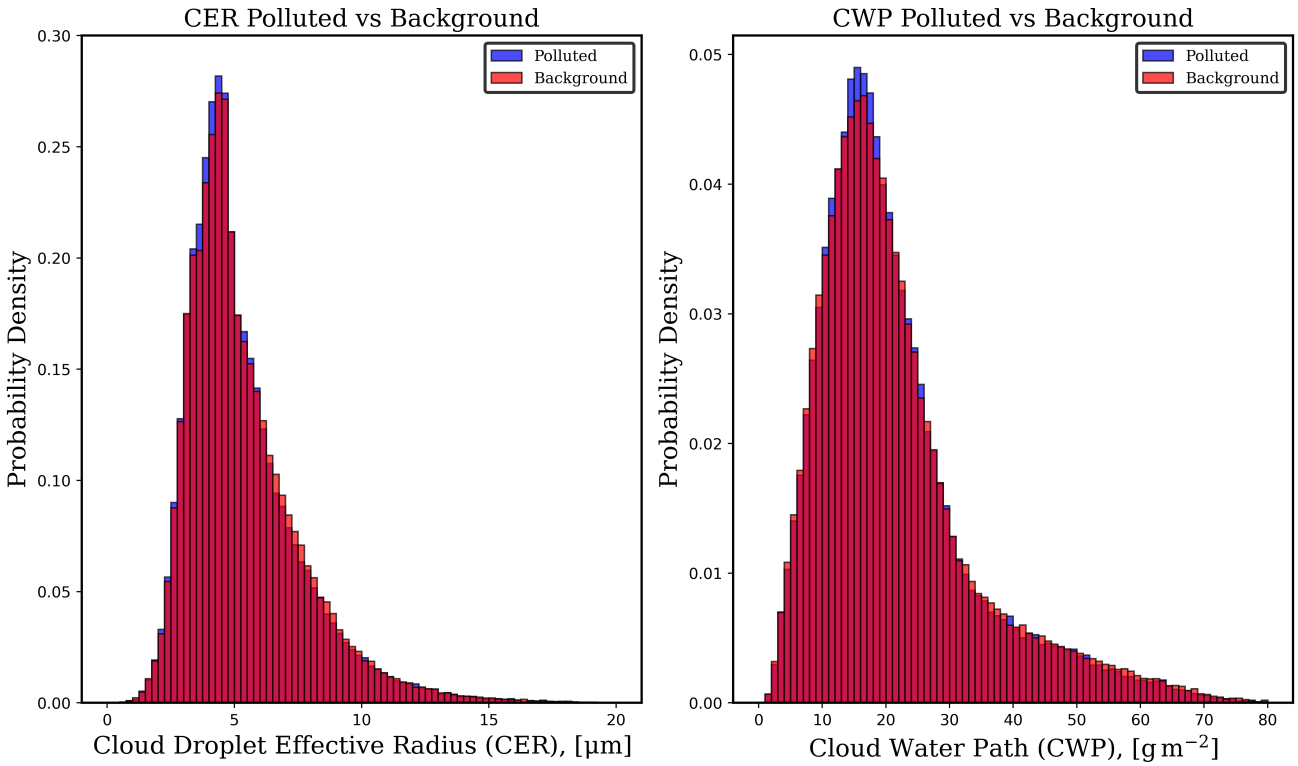

Figure 9: Comparison of polluted cloud properties to the background for the mass-filtered dataset. Subplots include (left to right) cloud water droplet effective radius and cloud liquid water path.